



ELSEVIER

Available online at [www.sciencedirect.com](http://www.sciencedirect.com)

SCIENCE @ DIRECT®

Nuclear Instruments and Methods in Physics Research A 540 (2005) 311–323

NUCLEAR  
INSTRUMENTS  
& METHODS  
IN PHYSICS  
RESEARCH  
Section A

[www.elsevier.com/locate/nima](http://www.elsevier.com/locate/nima)

# GRAPES-3—A high-density air shower array for studies on the structure in the cosmic-ray energy spectrum near the knee

S.K. Gupta<sup>a,\*</sup>, Y. Aikawa<sup>b</sup>, N.V. Gopalakrishnan<sup>a</sup>, Y. Hayashi<sup>b</sup>, N. Ikeda<sup>b</sup>, N. Ito<sup>b</sup>, A. Jain<sup>a</sup>, A.V. John<sup>a</sup>, S. Karthikeyan<sup>a</sup>, S. Kawakami<sup>b</sup>, T. Matsuyama<sup>b</sup>, D.K. Mohanty<sup>a</sup>, P.K. Mohanty<sup>a</sup>, S.D. Morris<sup>a</sup>, T. Nonaka<sup>b</sup>, A. Oshima<sup>b</sup>, B.S. Rao<sup>a</sup>, K.C. Ravindran<sup>a</sup>, M. Sasano<sup>b</sup>, K. Sivaprasad<sup>a</sup>, B.V. Sreekantan<sup>a</sup>, H. Tanaka<sup>b</sup>, S.C. Tonwar<sup>a</sup>, K. Viswanathan<sup>a</sup>, T. Yoshikoshi<sup>b</sup>

<sup>a</sup>HECR Group, Tata Institute of Fundamental Research, Homi Bhabha Road, Mumbai 400 005, India

<sup>b</sup>Graduate School of Science, Osaka City University, Osaka 558-8585, Japan

Received 17 August 2004; received in revised form 1 November 2004; accepted 10 November 2004

The GRAPES-3 Collaboration  
Available online 22 December 2004

---

## Abstract

The change in the spectral index from about  $-2.7$  to  $-3.1$  at  $\sim 3 \times 10^{15}$  eV in the all-particle energy spectrum of primary cosmic rays is very significant for learning about the nature of cosmic sources of ultra-high energy particles and their acceleration and propagation in the galactic disk. Any observation of a fine structure in the spectrum would be important for improving our understanding of these physical processes. The GRAPES-3 air shower array has been designed to achieve higher precision in determination of various shower parameters to enable observation of any fine structure in the energy spectrum, if it exists. The details of the shower detectors, shower trigger and the data acquisition system are presented here along with estimates of trigger efficiencies from Monte Carlo simulations for primary photons ( $\gamma$ -rays) and several nuclei.

© 2004 Elsevier B.V. All rights reserved.

PACS: 98.70.Sa; 96.40.Pq; 96.40.De; 98.70.Rz; 95.55.Vj; 13.85.Tp

Keywords: Cosmic rays; Extensive air showers; Composition; Energy spectra and interactions; Gamma-ray sources; Cosmic-ray detectors; Cosmic-ray interactions

---

\*Corresponding author. Tel.: +91 22 2280 4545; fax: +91 22 2280 4610.  
E-mail address: [gupta@grapes.tifr.res.in](mailto:gupta@grapes.tifr.res.in) (S.K. Gupta).

## 1. Introduction

A detailed understanding of the nature of cosmic-ray sources and processes accelerating charged particles to ultra-high energy (UHE),  $E \geq 10^{15}$  eV (PeV), still eludes us although considerable progress [1] has been made during recent years, on observational as well as theoretical fronts. Shock acceleration [2] through the well-known Fermi mechanism coupled with supernovae seem to offer a good solution at least up to PeV energies. Basically, the same mechanism has been extended to higher energies by invoking shocks progressing through stellar winds and acceleration through multiple shocks within the galactic disk. However, the observation of a change in the power law spectral index from about  $-2.7$  to  $-3.1$  at an energy  $\sim 3$  PeV called the *knee*, in the all-particle energy spectrum provides an important check on the details of various models [3] for particle acceleration and propagation.

For example, a change from an acceleration mechanism invoking supernova shock into the interstellar medium for energies below a PeV to supernova shock into the stellar wind of the progenitor star for higher energies has been suggested. Such a change would be accompanied by a change in the composition of cosmic-ray flux around the energy of the *knee*. A similar change could also be expected if the *knee* is mainly due to leakage of particles from the galactic disk when their Larmor radii become comparable to the thickness of the disk. The situation is considerably different in the case of the single-source model [4] which incorporates the effects due to a possible occurrence of a supernova in relatively recent past in the neighborhood of the Solar system. While a signature of the physical process responsible for the *knee* is being sought in the composition, it is also necessary to study the details of the energy spectrum around the *knee* to search for some fine structure [5,6] for the same purpose.

The electrons, in an air shower is the most studied component for getting information on the shower, particularly for generating trigger, determining arrival direction and estimating the energy of the primary particle. A measurement of the lateral (radial) density distribution of particles in a

shower using an array of unshielded charged particle detectors provides a good estimate of the observed number of particles in the shower,

$$N_e^{\text{obs}} = \int_{r_1}^{r_2} 2\pi r \rho_e(r) dr \quad (1)$$

where  $\rho_e(r)$  is the density of particles at a distance  $r$  from the core of the shower. With the core of the shower incident within the shower array,  $r_1$  is generally taken to be 0. The distance  $r_2$  depends on the size of the shower array but the observed lateral distribution function is generally extrapolated to  $r_2 = \infty$  to obtain the total number  $N_e^{\text{tot}}$  of particles in the shower. Despite considerable fluctuations in the development of individual showers in the atmosphere and the differences in development profile for different primary nuclei, the shower size ( $N_e^{\text{obs}}$  or  $N_e^{\text{tot}}$ ) is known to be a good parameter for estimating primary energy of showers.

Practical constraints limit the number of detectors employed in a shower array, thus providing only a sampling of the particle density  $\rho_e(r)$  at a limited number of points. Even in good shower arrays, for example, the CASA [7], the Tibet  $AS\gamma$  [8] and the KASCADE [9] arrays, the detection area does not exceed a few percent of the physical area over which the array is spread out. However, this is an important parameter which contributes significantly to the accuracy of measurement of shower size (and consequently primary energy) as well as the arrival direction, particularly for UHE  $\gamma$ -ray astronomy. The shower size and therefore the optimum density of the detectors is also dependent on the observational level. It is quite important to have higher density of detectors to achieve larger triggering efficiency for lower energy showers. The MILAGRO [10] experiment is attempting to achieve full particle detection sensitivity over a large area by instrumenting a 8 m deep water pond of  $80 \times 60 \text{ m}^2$  area with two layers of photomultiplier tubes. On the other hand, the ARGO-YBJ collaboration [11] is installing an array of resistive plate counters fully covering an area of  $74 \times 78 \text{ m}^2$  surrounded by 50% coverage over an area of  $100 \times 100 \text{ m}^2$ .

With similar considerations in mind, the GRAPES-3 shower array [12] has been designed

to have one of the most compact configurations of conventional type arrays with only 8 m separation between adjacent detectors which are arranged in a symmetric hexagonal geometry. While the final aim is to have 15 rings with 721 detectors, covering a distance of up to 120 m from the center of the array, observations have started in early 2000 with 217 detectors located within the inner 8 rings. The GRAPES-3 experiment is located at Ooty (11.4°N latitude, 76.7°E longitude and 2200 m altitude), a popular mountain resort town in southern India.

The design of a typical density detector of the GRAPES-3 array along with its performance is described in Section 2. The details of the shower trigger system and the main features of the data acquisition system are also presented in this section. A few interesting observational results are also contained in Section 2. Detailed Monte Carlo simulations have been carried out for estimating the trigger efficiency as a function of primary energy for various primary nuclear groups. Salient features of these simulations along with some of the significant results are discussed in Section 3. In view of the fact that the unshielded charged particle detectors of the GRAPES-3 array detect not only electrons, muons and charged hadrons but also high energy photons ( $\gamma$ -rays), simulations have been carried out to estimate the contribution of  $\gamma$ -rays to observed ‘particle’ densities as a function of the core distance. The details of these simulations and some of the results are presented in Section 4 followed by a brief summary in Section 5.

## 2. GRAPES-3 air shower array

In Fig. 1 a schematic layout of the GRAPES-3 array is shown. A total of 721 detectors are planned to be installed over a period of time, depending on the availability of plastic scintillators which are being fabricated in-house. Presently 288 detectors are operational. However here, data with only 217 detectors has been used. Fig. 1 also shows 16 squares in the north-west region. Each of these squares represents a 4-layer muon tracking detector with an energy threshold of 1 GeV for vertical muons. Each layer consists of 58 proportional

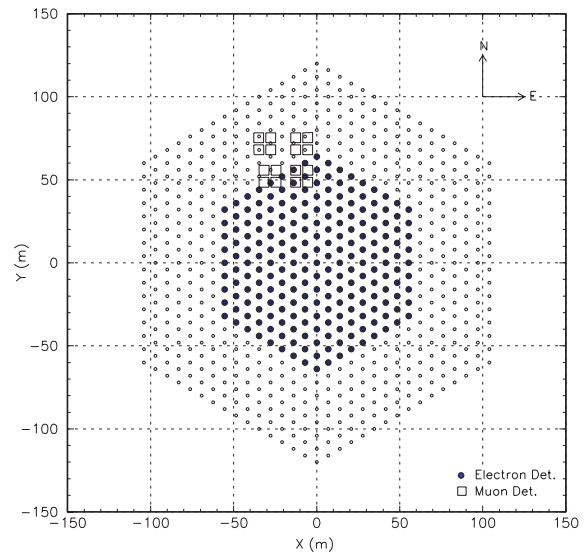


Fig. 1. Schematic layout for the 721 detector (open circles  $\circ$ ) GRAPES-3 shower array of which 217 detectors (filled circles  $\bullet$ ) used at present are shown. Each of the 16 squares ( $\square$ ) represents a 35m<sup>2</sup> area muon tracking detector with  $E_{\mu} \geq 1$  GeV.

counters, each 6 m long with  $10 \times 10$  cm<sup>2</sup> cross-sectional area. This large area, muon detector has been designed for studies [13] on the composition of primary cosmic rays and studies on cosmic sources of UHE  $\gamma$ -rays. Large area muon detector is also required for observations on muons produced by lower energy protons [14] which are affected by phenomena occurring on the Sun, such as solar flares and coronal mass ejections leading to magnetic disturbances around the Earth. The details of the muon detector and its performance in relation to these physics objectives is discussed elsewhere [15]. The actual physical layout of the electron detectors, the central control room and the halls housing the muon detector may be seen in Fig. 2 which also shows the slight slope in the ground in the east–west direction.

### 2.1. Shower detector

Each shower detector consists of 4 blocks of plastic scintillators, each 5 cm thick and  $50 \times 50$  cm<sup>2</sup> in area, placed inside a square aluminum tank as shown in Fig. 3. A 5 cm diameter



Fig. 2. A view of the GRAPES-3 array showing electron detectors and the central control room. Four halls housing the muon detectors are seen on the left. The detectors lined up from the top-right to the bottom-left in the picture, are along the East to West direction.

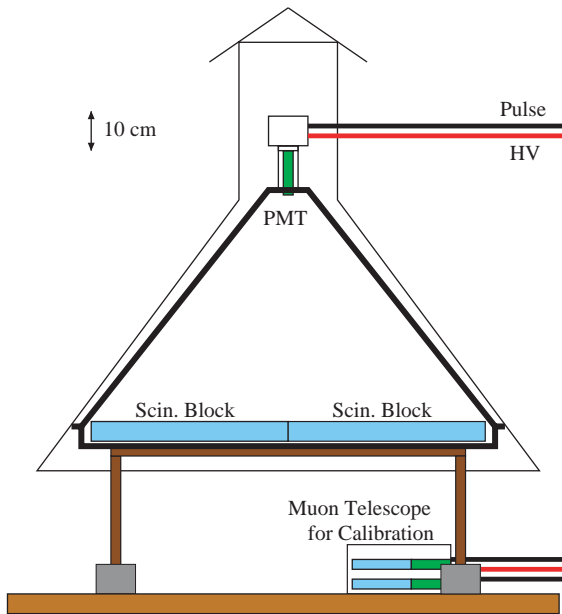


Fig. 3. Schematic of a shower detector, including the muon telescope under the detector, used for calibration.

photomultiplier tube (PMT) model ETL9807B is mounted on top of a trapezoidal-shaped aluminum cone, with its face at a height of 60 cm above the scintillator surface. The inner surfaces of the tank and the cone have been painted with super-white ( $\text{TiO}_2$ ) paint to increase the efficiency for collection of diffuse photons at the PMT. The whole detector assembly is covered by a large

aluminum cone to protect it from rain and heating due to direct sunlight. The detector is mounted on a 40 cm height stand, as shown in Fig. 3, to raise it well above flowing rain water. This arrangement allows, a small muon telescope as shown in Fig. 3, to be placed under the detector for single particle (muon) calibration as discussed below.

## 2.2. Shower detector calibration

As shown in Fig. 3, shower detectors are calibrated using a small muon telescope made of two independent scintillator pedals (each  $15 \times 15 \text{ cm}^2$  in area and 5 cm in thickness) placed inside an aluminum box with a vertical separation of 5 cm between them. Each being fully sensitive to the passage of minimum-ionizing particles, a 2-fold 100 ns coincidence between the two scintillators selects almost all muons with zenith angle  $\theta \lesssim 50^\circ$ . Most of these muons pass through the shower detector located above the muon telescope, thus providing the distribution of integrated-charge for the passage of minimum-ionizing particles. Typical single-particle response for four detectors in terms of the distribution of integrated-charge (ADC value) is shown in Fig. 4. The

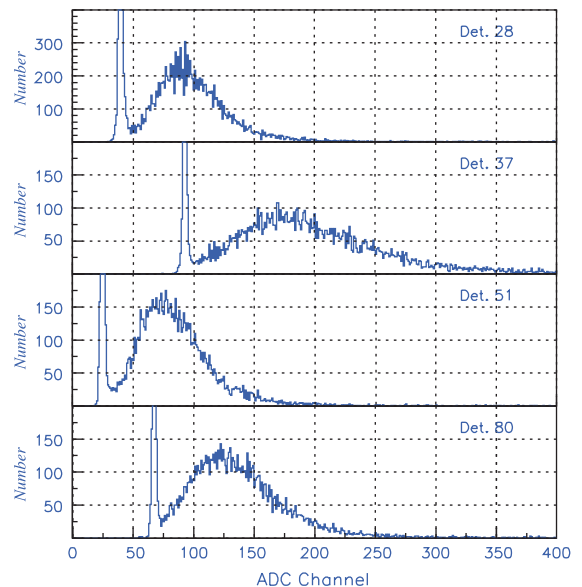


Fig. 4. Typical distributions of the integrated-charge (ADC value) for single particles (muons) for 4 shower detectors.

calibration distribution for each detector is used to convert the signal observed in a shower to ‘equivalent’ number of particles. The spatial non-uniformity in the response of the detector to single particles arises due to differences in the scintillation efficiency from block to block and due to geometrical effects. However, all detectors have been designed to have a response, which is uniform within  $\sim 10\%$ , over its  $1\text{ m}^2$  area.

The high voltage for each detector PMT has been adjusted to give a most probable ADC value of about 25 counts for a minimum-ionizing particle. A 15-bit dynamic range, 32 channel, charge integrating ADC (CAEN model C205N) used in the experiment allows, measurement of a maximum density of  $\sim 1000$  particles. However, the response of the PMT output becomes non-linear for signals  $\gtrsim 200$  particles. However, this limitation in the dynamic range of the PMTs does not affect measurement of showers of energies  $\lesssim 10\text{ PeV}$  except for detectors located within  $\sim 10\text{ m}$  from the shower core.

The arrival time of PMT output is measured to a precision of 0.3 ns, the uncertainty in the arrival time due to photon collection at the PMT is  $\sim 1\text{ ns}$ . However, the time resolution is dominated by the spread in the arrival time of shower particles at the detector which is  $\sim 3\text{ ns}$ . This limitation is largely overcome by a high density of deployment of detectors to achieve a good angular resolution ( $\lesssim 1^\circ$ ) for showers of energy  $\sim 100\text{ TeV}$  ( $1\text{ TeV} = 10^{12}\text{ eV}$ ). The accuracy in angle determination improves with increasing primary energy.

### 2.3. Shower trigger

The anode pulse from each shower detector is taken to the central control room using a 230 m long,  $50\ \Omega$  impedance RG-58 cable. It is then passively split into 2 pulses, first pulse is attenuated down to 3% of its original amplitude and then a.c. coupled to a channel of ADC module through an additional cable delay (80 m,  $50\ \Omega$  impedance RG-174). The second pulse is amplified (16-channel, Phillips Scientific amplifier, Model 776) by a factor of 10 before being fed to a discriminator (16-channel, Phillips Scientific Model 706) set at a threshold of  $-30\text{ mV}$ . One of the

NIM outputs of the discriminator goes to a channel of the TDC (16-channel, Hoshin Model C021 or Phillips Scientific Model 7186) while the other output goes for shower selection as well as to the rate monitoring system (Fig. 5).

In order to achieve a low-energy threshold for the trigger, a simple 3-line coincidence has been used to generate the Level-0 trigger, as shown in Fig. 6, which acts as GATE for the ADCs and START for the TDCs. Looking at the detectors lined up in the north–south direction, the signals from the discriminators for all the detectors in a given line are OR’ed together. Then a 100 ns wide, 3-fold coincidence is generated among the line OR’s for each combination of three adjacent lines. All these 3-line coincidences, (L1.L2.L3), (L2.L3.L4), (L3.L4.L5), etc., are OR’ed together to generate the Level-0 trigger. Note that only the inner 6 rings (detectors 001 to 127) of the 8 rings have been used for generating the line OR’s in order to optimize the selection of showers with cores incident within the array. The observed level-0 trigger rate is 52 Hz.

Despite selection of showers based on 3-line trigger, the distribution of shower cores is expected to be uniform because of the unrestrictive nature of this trigger as explained below. Expectedly, the 3-line trigger selects a significant number of small but local showers and also very large showers whose cores are far away. Therefore an additional condition has been imposed on the shower selection, namely a requirement that at least ‘ $n$ ’ out of 127 detectors should have triggered the discriminators within  $1\ \mu\text{s}$  using relatively slow EPROMS. The observed shower rate for this Level-1 trigger is  $\sim 13\text{ Hz}$  for a value of  $n = 10$  used in the experiment.

To study the effect of trigger selection on the distribution of shower cores, Monte Carlo simulations have been carried out using primary protons in the energy range  $1\text{ TeV}–3\text{ PeV}$ , on a power law spectrum ( $-2.7$ ) with zenith angle  $\theta < 50^\circ$ . The simulated showers were allowed to land uniformly over the entire area covered by the 217 detectors which is represented by the outer hexagon in Fig. 7. A scatter plot of the core locations of  $10^4$  showers that satisfy the requirements for shower selection (namely Level-0 and Level-1 triggers) is

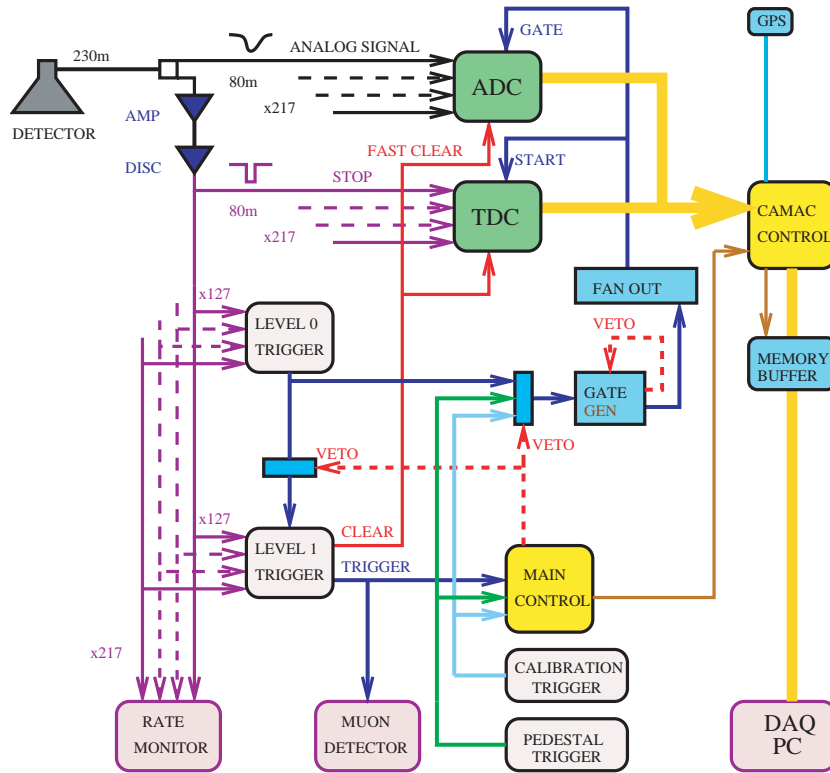


Fig. 5. Schematic of the signal processing system for pulses received from the PMTs of the shower detectors to generate the signals sent to ADCs and TDCs as well as the signals used for generating the shower trigger and rate monitoring. Basic elements of the data acquisition system are also shown.

also shown in Fig. 7. The inner hexagon represents the boundary of the 127 detectors used in generation of the trigger. Since the Level-1 trigger does not impose any location dependent selection, the shower cores have a uniform distribution except for the edge effects. In the analysis of data the drop in the selection efficiency towards the edge of the shower array, based on the results from these simulations, which are energy-dependent, are taken into account.

#### 2.4. Data acquisition system

The data acquisition system is a modified CAMAC-based system using crate controllers which are designed and fabricated in-house. A fast trigger, within 200 ns after the arrival of a shower is required to initiate the digitization in the ADCs and TDCs and the Level-0 trigger is used to

serve this objective. In addition a large number of local, small-size showers that get selected by the Level-0 trigger are eliminated by the Level-1 trigger. In addition to the pulse charge recorded for shower detectors with ADCs and the pulse arrival time recorded with TDCs, the absolute time (local time) of the shower is also recorded to a precision of  $1\ \mu\text{s}$  for each Level-1 trigger. A 10 MHz temperature-stabilized quartz crystal oscillator has been used in the real-time clock which is corrected every second with a signal from a GPS receiver. For each Level-1 trigger, nearly 1500 bytes of data are transferred to a 32 KB buffer of a dual-memory buffer. When the first 32 KB buffer gets filled, the stored data is transferred into the hard disk of data acquisition PC. In the meantime a switching signal routes the incoming data to the second 32 KB buffer to prevent any loss of data. The data from the hard disk are periodically

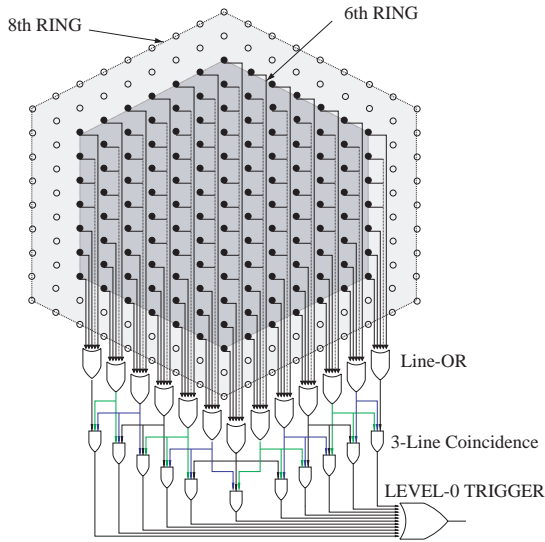


Fig. 6. Schematic of the shower trigger system for generating the Level-0 trigger using the basic 3-line coincidence from among the inner 127 detectors (6 rings).

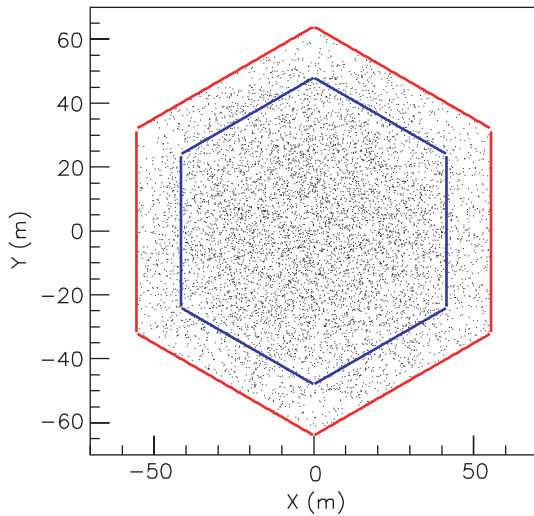


Fig. 7. Core distribution of simulated proton showers (1 TeV–3 PeV,  $\theta < 50^\circ$ ) that trigger the system. Inner hexagon contains 127 detectors (6 rings) used in trigger and outer hexagon contains all 217 detectors (8 rings).

transferred to CD/DVD for permanent storage. The dead-time of the data acquisition system is only 3.1 ms. Note that the ADCs and TDCs are triggered by the Level-0 trigger but are fast-cleared

within the next  $2.5\ \mu\text{s}$  if the Level-1 trigger does not get generated.

A plot of the observed signals in the detectors for a typical shower is shown in Fig. 8. The height of the bar for each detector represents the number of ‘equivalent particles’ observed in that detector. The tallest bar nearly coincides with the location of the shower core. The distribution of the number of TDC channels triggered for Level-1 trigger is shown in Fig. 9. Note that the mean number of TDC channels triggered is quite large  $\sim 33$ , although the number required in the selection is only 10. However, in about 0.5% of the recorded showers, the number of TDC channels triggered is  $< 10$ . This deficit is due to the fact that Level-1 is a slow trigger that requires a coincidence over a broad time interval of  $1\ \mu\text{s}$ . In contrast the TDCs record the arrival time of signals over a narrower time interval of  $\sim 500\ \text{ns}$ . Therefore, if an accidental pulse, unrelated to the shower arrives at a time, outside the TDC acceptance window but inside the Level-1 window, it would not be recorded as a valid TDC count. The observed trigger rate  $\sim 0.5\%$  of deficient showers, where the number of TDC channels is  $< 10$ , is consistent with

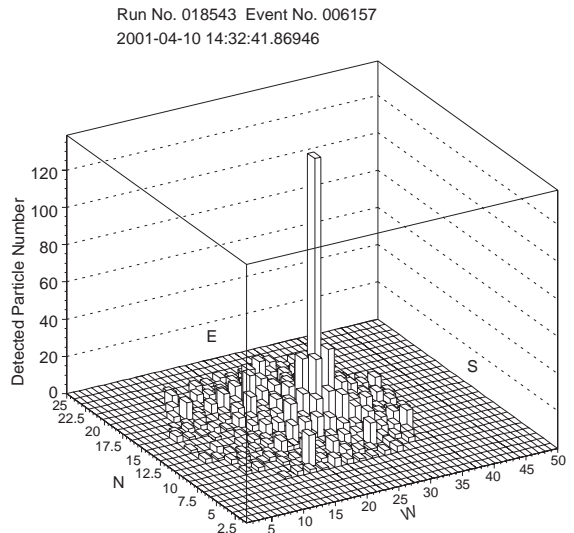


Fig. 8. A plot of the observed signals from the detectors for a typical shower. The length of the bar for each detector represents the number of ‘equivalent’ particles observed in the detector. The tallest bar nearly coincides with the location of the shower core.

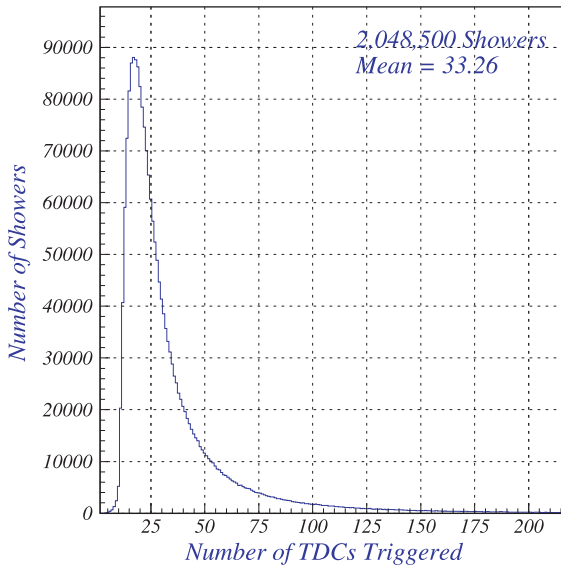


Fig. 9. The observed distribution of the number of TDC channels triggered for the Level-1 trigger.

observed individual detector counting rates of 300–2000 Hz. In addition, relevant atmospheric parameters, such as barometric pressure, temperature, humidity, rain, wind speed and wind direction are also recorded once every minute by an independent weather station.

### 2.5. Rate monitoring

The stability of the response of shower detectors is an important parameter in ensuring a stable energy threshold for the trigger. While single particle calibrations as discussed above (Section 2.2) are taken about once a month, the counting rate for each detector is recorded for every 100 ms using the output pulse from the discriminator through the ‘RATE MONITOR’ system (Fig. 5). This is an independent data recording system which has been designed to look for short term transients and correlation of detector rates with atmospheric parameters.

In Fig. 10 variation in the rates for three of the 217 detectors namely detector numbers 06, 16 and 30 over a period of seven days during 15–22 February 2001 along with the variations in the shower trigger rate (Level-1), the atmospheric

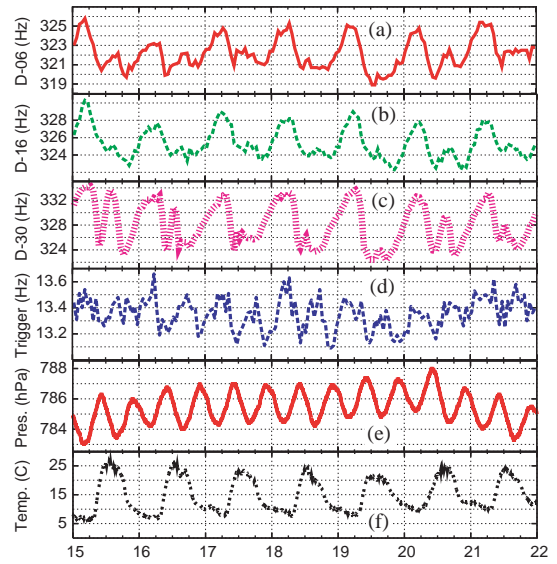


Fig. 10. Observed variation in counting rates for three shower detectors; (a) D-06, (b) D-16 and (c) D-30, recorded using the rate monitoring system. The variation in; (d) the shower trigger rate, (e) the atmospheric pressure and (f) the temperature are shown for the period of seven days during 15–22 February 2001.

pressure and the temperature are shown. As expected the temperature shows diurnal variation in phase with solar radiation received on ground as seen in Fig. 10f. However, the pressure data as seen from Fig. 10e shows periodic variation of two cycles per day.

It is to be noted that the three detector rates (Figs. 10a–c) also show periodic variations of two cycles per day, but with a second peak of significantly smaller amplitude. This observation may be understood in terms of the thermal properties of the scintillation detectors and their response to varying atmospheric pressure. A major fraction of the detector rate variation seen in Fig. 10a–c is due to a negative temperature coefficient of the scintillator and the PMT assembly and a smaller fraction is due to the varying absorption of charged particles in the atmosphere. It is interesting to note that the shower trigger rate (Fig. 10d) also shows a periodic variation of two cycles per day but in opposite sense to the pressure change (Fig. 10e).

The pressure wave is produced by a complex interaction of solar heating and the nonlinear

response of the upper atmosphere to this forcing. It is well-known that the amplitude of the pressure wave depends on the latitude of the site and is larger at lower latitudes [16]. The low latitude location ( $11.4^\circ\text{N}$ ) of Ooty is responsible for the sizable 12 h periodicity seen in the pressure data (Fig. 10e).

The sensitivity of the GRAPES-3 experiment can be gauged from the fact that a small amplitude ( $\sim 1\text{ hPa}$ ) of the pressure wave ( $\sim 0.2\%$ ) significantly modulates the observed rate of showers ( $\sim 1\%$ ). For the sake of clarity the Level-1 shower trigger rate and the pressure data are plotted separately in Fig. 11. A strong anti-correlation between the two parameters is clearly visible. The pressure data shows that the highest values are reached at about 10 h and 22 h local time when the shower trigger rates reach their minimum values. The coefficient of the anti-correlation is  $\sim 80\%$ . This anti-correlation can be explained in terms of a change in the atmospheric absorption of cosmic ray showers due to the pressure wave. This feature of the GRAPES-3 experiment is expected to be of critical importance in studying various transient phenomena including those of cosmic, solar or

atmospheric origin. The pressure effect is also clearly seen in the muon counting rate which will be described elsewhere [13].

### 3. Shower trigger efficiency—Monte Carlo simulations

Since one of the main objectives of the GRAPES-3 experiment is an accurate measurement of the primary energy spectrum around the *knee* region and also its extension to the lowest possible energies in order to have some overlap with direct measurements with satellite and balloon-borne experiments [17–19], it is important to study the energy threshold of shower trigger, for different incident primary particles under trigger conditions described in Section 2.3. This has been carried out using showers simulated with the CORSIKA [20,21] package using the QGSJet model [22] for hadronic interactions. The detector response in the simulations is treated by generating an equivalent signal in each detector based on the observed distribution for minimum-ionizing particles as shown in Fig. 4.

In order to take into account the contribution of  $\gamma$ -rays to the response of the 5 cm thick scintillator used for shower detectors, showers have been generated using the EGS package thus recording all the electrons and  $\gamma$ -rays ( $E > 1\text{ MeV}$ ) reaching the observational level of  $800\text{ g cm}^{-2}$ . Showers have been generated over a wide range of energies, 1–300 TeV, for four different types of primary particles,  $\gamma$ -rays, protons, helium and iron nuclei. The increase in the triggering efficiency with increasing primary energy is shown in Fig. 12. As expected, the efficiency is highest for  $\gamma$ -ray primaries at a given energy, reaching almost 90% at  $E_\gamma \sim 30\text{ TeV}$ , followed by showers initiated by protons which reach the same efficiency at  $E_p \sim 50\text{ TeV}$ .

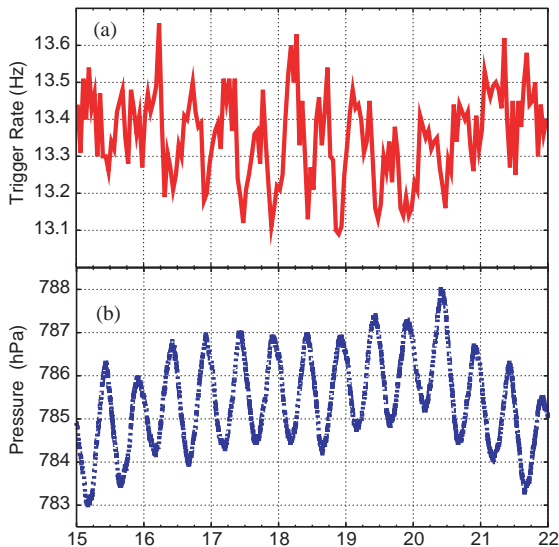


Fig. 11. (a) The observed variation in shower rate and (b) the atmospheric pressure for the period of seven days during 15–22 February 2001. A 12-h periodicity is seen in the pressure and in the shower rate data. A high degree of anti-correlation between pressure and shower rate is clearly visible.

### 4. Monte Carlo simulations—response to $\gamma$ -rays in showers

As mentioned above, the use of 5 cm thick plastic scintillator for the shower detector makes it sensitive to large flux of low energy  $\gamma$ -rays which

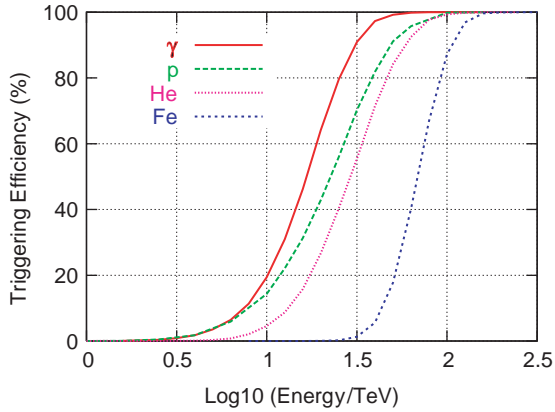


Fig. 12. Variation in efficiency of level-1 trigger as a function of primary energy for showers initiated by primary  $\gamma$ -rays, protons, helium and iron nuclei with the zenith angle,  $\theta < 25^\circ$  and the core inside the 6th ring of detectors. Showers have been simulated with the CORSIKA package using the QGSJet model for hadron interactions and the EGS option for electrons and  $\gamma$ -rays.

accompany the electrons in showers. Therefore the response of these detectors has been studied [23] using  $\gamma$ -rays from simulated showers and the GEANT4 package. The virtual shower detector used in GEANT4 is shown in Fig. 13, including a trapezoidal-shaped, aluminum cover used to protect the detector from rain. Also shown inside the rain cover is a second trapezoidal-shaped aluminum cone and tank assembly which houses the four scintillators (each  $50\text{ cm} \times 50\text{ cm} \times 5\text{ cm}$ ) in a light-tight environment as described in Section 2.1. The four scintillators are clearly visible as thin square blocks at the bottom of the cone and tank assembly. Below the scintillators is a mild steel structure with four legs to position the detector 40 cm above the ground. The four larger square legs seen near the bottom of Fig. 13 are part of a concrete structure that anchors the detector to the ground. Finally, the four large blocks seen at the bottom of Fig. 13 represent the soil below the detector, which is also used in GEANT4 simulation to provide a realistic reproduction of the detector and its surrounding material. A charged particle track and its interaction products are also shown in Fig. 13.

A total of  $5 \times 10^6$   $\gamma$ -ray,  $2 \times 10^6$  electron and  $2 \times 10^6$  muon events have been generated for

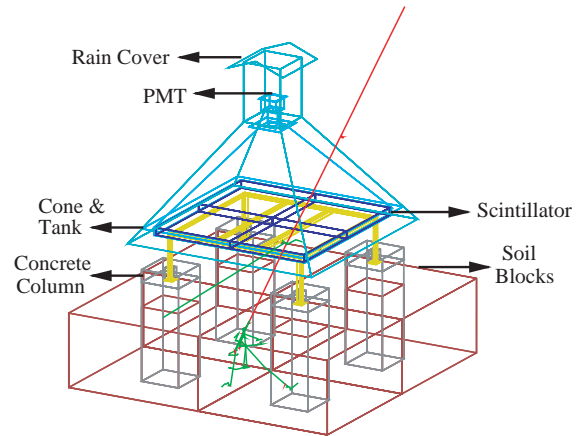


Fig. 13. Virtual scintillation detector of the GRAPES-3 array constructed for use in GEANT4 package. Outer and inner trapezoidal-shaped, rain cover and cone& tank assembly respectively, are indicated by arrows. Also seen are four scintillator blocks each  $50\text{ cm} \times 50\text{ cm} \times 5\text{ cm}$  in size and the PMT housing as indicated by arrows.

studying the response of the shower detector. Their energies have been distributed uniformly between 1 MeV and 10 GeV for  $\gamma$ -rays and electrons and between 10 MeV and 100 GeV for muons on a logarithmic scale. The particles are randomly projected on the scintillator from a direction with zenith angle varying from  $0^\circ$  to  $60^\circ$  and azimuthal angle from  $0^\circ$  to  $360^\circ$ . The program determines the energy deposited in the scintillator for each incident particle. The mean energy deposited as a function of the energy of the incident particle is shown in Fig. 14 separately for  $\gamma$ -rays (top), electrons (middle) and muons (bottom), for a range of zenith angles. Each of these distributions has been fitted by a two-dimensional function of particle energy and  $\sec(\theta)$  as shown in Fig. 14. These functions are then used for calculating the detector response to the passage of  $\gamma$ -rays, electrons and muons in a shower simulated using the CORSIKA package as described above in Section 3.

The average lateral distribution for  $\gamma$ -rays, electrons and muons in showers initiated by protons of primary energy 300 TeV, arriving in vertical direction is shown in Fig. 15. It is to be noted that the number of  $\gamma$ -rays of energy  $> 10\text{ MeV}$  at a distance of 50 m from the core is

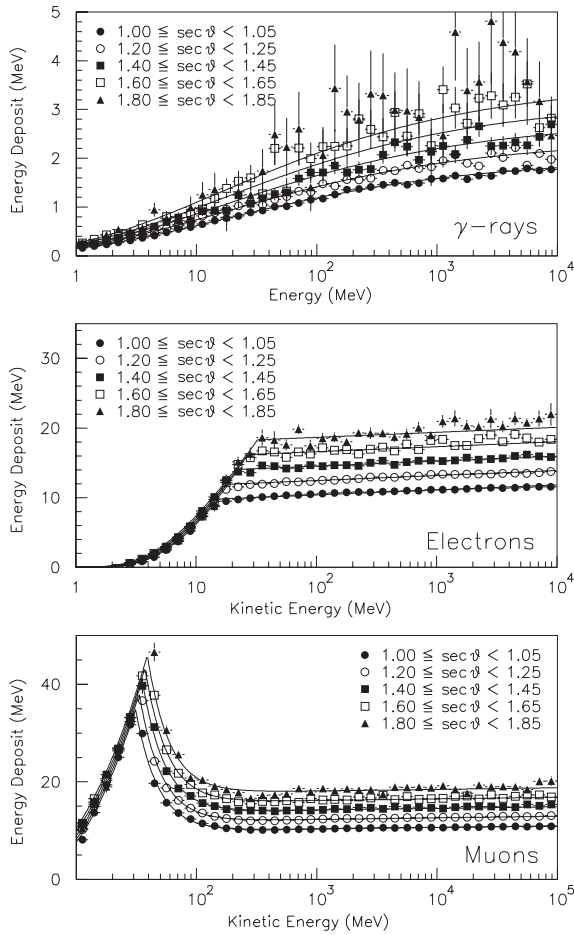


Fig. 14. The mean energy deposited as a function of the energy of the incident particle shown separately for  $\gamma$ -rays (top), electrons (middle) and muons (bottom), for a range of zenith angle, expressed as  $\sec(\theta)$ .

about 5 times higher than the number of electrons of the same energy. Fig. 16 shows the average lateral distribution in terms of the energy deposited in the scintillator due to  $\gamma$ -rays, electrons and muons respectively for the same set of 300 TeV showers. This was done by using the particle density shown in Fig. 15, and the energy deposition functions obtained from Fig. 14 separately for each of the three components, namely  $\gamma$ -rays, electrons and muons.

It is seen from Fig. 16 that the energy deposited due to muons can be easily neglected as it is relatively small compared to the deposition due to

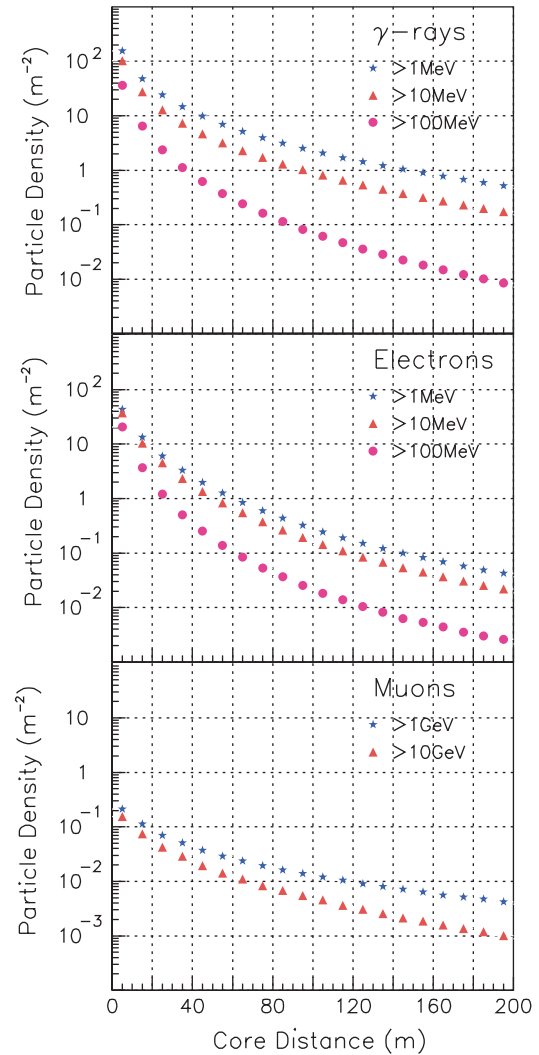


Fig. 15. Average lateral distribution for  $\gamma$ -rays, electrons and muons in showers initiated by vertical protons of primary energy of 300 TeV.

the electrons up to distances  $\sim 100$  m. However, the energy deposited due to  $\gamma$ -rays must be properly taken into account since it adds  $\sim 30\%$  to the energy deposited by the electrons near the core, and increasing slowly to  $\sim 70\%$  at 100 m from the core. This is equivalent to a flattening of the lateral distribution of electrons which leads to an over-estimate of the shower size by  $\sim 10\%$ . The contribution due to  $\gamma$ -rays also depends on the nature of the primary particle. This factor has to

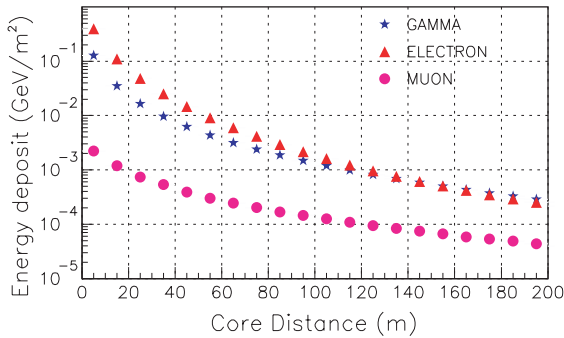


Fig. 16. Average lateral distribution for the energy deposited in the scintillator due to  $\gamma$ -rays, electrons and muons obtained using the numbers shown in Fig. 15 and the energy deposition functions obtained from Fig. 14.

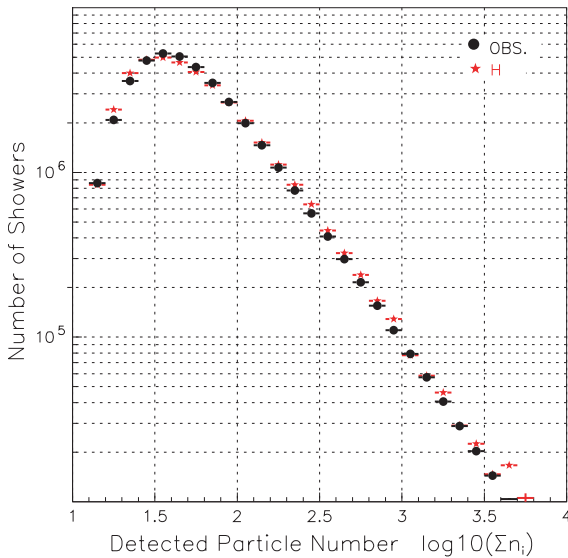


Fig. 17. A comparison of the observed distribution of the ‘particle-sum’, over the 217 detectors for showers collected over a period of 40 days, with the distribution expected for simulated showers for proton primaries. Showers were generated (CORSIKA with QGSJet model) assuming a differential power-law energy spectrum,  $N(E)dE \sim E^{-2.7}dE$ , over the 1 TeV–1 PeV energy range. The expected distribution is normalized to the total number of observed showers.

be considered when comparing the shower size estimated from a simple application of the Nishimura–Kamata–Greisen (NKG) [24,25] relation and the size determined from a complete CORSIKA simulation using the EGS package.

A comparison of the observed distribution of the ‘particle-sum’ over 217 detectors with the expected distribution for showers, including the detector response as discussed above, but only for protons as primary particles is shown in Fig. 17. It is interesting to note that the simulations reproduce the observations reasonably well, provided the contribution of the low energy  $\gamma$ -rays to the scintillation detectors is also included in carrying out the simulations.

## 5. Summary

The GRAPES-3 array has become operational in March 2000 with 217 density detectors arranged in a compact hexagonal configuration with inter-detector spacing of only 8 m. The 3-line trigger rate is 52 Hz which is reduced to 13 Hz when a minimum of 10 detectors are required to be triggered in order to be able to reconstruct the arrival direction of the shower. Several of the observed features of showers have been reproduced well, by Monte Carlo simulations which show that the detection energy threshold for showers to be  $\sim 50$  TeV for proton primaries at 90% triggering efficiency. Simulation studies have also shown that the shower size may be determined with an accuracy of  $\sim 10\%$  at  $10^{4.5}$  particles with the GRAPES-3 array.

## Acknowledgements

We thank D.B. Arjunan, K. Manjunath, B. Rajesh and C. Ravindran for the testing, installation and operation of various detector and electronic modules. The administrative services of V. Viswanathan during all phases of the experiment are gratefully acknowledged. It is a pleasure to thank A.A. Basha, G.P. Francis, I.M. Haroon, V. Jeyakumar, A. Pushpanathan and K. Ramadass for their help in the fabrication, assembly and installation of various mechanical components and detectors. We also thank M.A. Ali, P. Amalraj, M. Iyer, B. Jasper, G.C. Kamat, A. Pratheep, T.T. Sreedevi and S. Thirunavukkarasu for their help in certain phases of the experiment. The Japanese

members of the GRAPES-3 collaboration wish to acknowledge the partial financial support from the Ministry of Education of the Government of Japan for the experiment.

## References

- [1] V.S. Berezinskii, et al., *Astrophysics of Cosmic Rays*, North-Holland, Amsterdam, 1990.
- [2] P.L. Biermann, T.K. Gaisser, Todor Stanev, *Phys. Rev. D* 51 (1995) 3450.
- [3] S.C. Tonwar, *Nucl. Phys. B (Proc. Suppl.)* 122B (2003) 109.
- [4] A.D. Erlykin, A.W. Wolfendale, *J. Phys. G* 23 (1997) 979.
- [5] G. Schatz, *Astropart. Phys.* 17 (2002) 13.
- [6] S.K. Gupta, et al., *Phys. Rev. D* 68 (2003) 052005.
- [7] A. Borione, et al., *Nucl. Instr. and Meth. A* 346 (1994) 329.
- [8] M. Amenomori, et al., *Nucl. Instr. and Meth. A* 288 (1990) 619.
- [9] T. Antoni, et al., *Nucl. Instr. and Meth. A* 513 (2003) 490; T. Antoni, et al., *Astropart. Phys.* 14 (2001) 245.
- [10] R. Atkins, et al., *Nucl. Instr. and Meth. A* 449 (2000) 478; R. Atkins, et al., *Astrophys. J.* 595 (2003) 803.
- [11] C. Bassi, et al., *Nucl. Instr. and Meth. A* 443 (2000) 342; C. Bassi, et al., *Astropart. Phys.* 17 (2002) 151.
- [12] N. Ito, et al., *Proceedings of the 25th ICRC, Durban*, vol. 7, 1997, p. 225; Y. Hayashi, et al., *Proceedings of the 26th ICRC, Salt Lake City*, vol. 1, 1999, p. 236.
- [13] Y. Hayashi, et al., *Proceedings of the 26th ICRC, Salt Lake City*, vol. 1, 1999, p. 276.
- [14] S. Kawakami, et al., *Proceedings of the 26th ICRC, Salt Lake City*, vol. 7, 1999, p. 171; Y. Hayashi, et al., *Proceedings of the 27th ICRC, Hamburg*, vol. 1, 2001, p. 111; S. Kawakami, et al., *Proceedings of the 27th ICRC, Hamburg*, vol. 9, 2001, p. 3473; H. Kojima, et al., *Proceedings of the 27th ICRC, Hamburg*, vol. 10, 2001, p. 3943; T. Nonaka, et al., *GRAPES-3 Preprint 2004c*, to be published.
- [15] Y. Hayashi, et al., preprint, 2004, to be published.
- [16] S. Chapman, R.S. Lindzen, *Atmospheric Tides: Thermal and Gravitational*, Gordon & Breach Science, 1987.
- [17] K. Asakimori, et al., *Astrophys. J.* 502 (1998) 278.
- [18] A.V. Apanasenko, et al., *Astropart. Phys.* 16 (2001) 13.
- [19] J.P. Wefel, et al., *J. Phys. G: Nucl. Part. Phys.* 29 (2003) 821.
- [20] J.N. Capdevielle, et al., *The Karlsruhe Extensive Air Shower Simulation Code CORSIKA*, Kernforschungszentrum Karlsruhe KfK 4998, 1992.
- [21] D. Heck, et al., *CORSIKA: A Monte Carlo Code to Simulate Extensive Air Showers*, Forschungszentrum Karlsruhe FZKA 6019, 1998; D. Heck, et al., *Proceedings of the 27th ICRC, Hamburg*, 2001, p. 233.
- [22] N.N. Kalmykov, S.S. Ostapchenko, A.I. Pavlov, *Nucl. Phys. B (Proc. Suppl.)* 52B (1997) 17.
- [23] T. Yoshikoshi, et al., *Proceedings of the 27th ICRC, Hamburg*, vol. 2, 2001, p. 612.
- [24] K. Kamata, J. Nishimura, *Prog. Theor. Phys. Suppl.* 6 (1958) 93; J. Nishimura, *Handbuch der Physik*, vol. 46-2, Springer, Berlin, 1967, p. 1.
- [25] K. Greisen, *Annu. Rev. Nucl. Sci.* 10 (1960) 63.